Supporting Information

Spin Blockades to Relaxation of Hot Multi-Excitons in Nanocrystals

Tufan Ghosh[a], Joanna Dehnel[b], Marcel Fabian[a], Efrat Lifshitz[b], Roi Baer[a] and Sanford Ruhman[a]

a) Fritz Haber Center for Molecular Dynamics and the Institute of Chemistry, The Hebrew University of Jerusalem, Jerusalem 9190401, Israel.
b) Schulich Faculty of Chemistry, Solid State Institute, Russell Berrie Nanotechnology Institute, Nancy and Stephen Grand Technion Energy Program, and Department of Materials Science and Engineering, Technion Israel Institute of Technology, Haifa 3200003, Israel.

sandy@mail.huji.ac.il (S.R.), roi.baer@huji.ac.il (R.B.), and efrat333@gmail.com (E.L.)

Determining the spin flip time constant

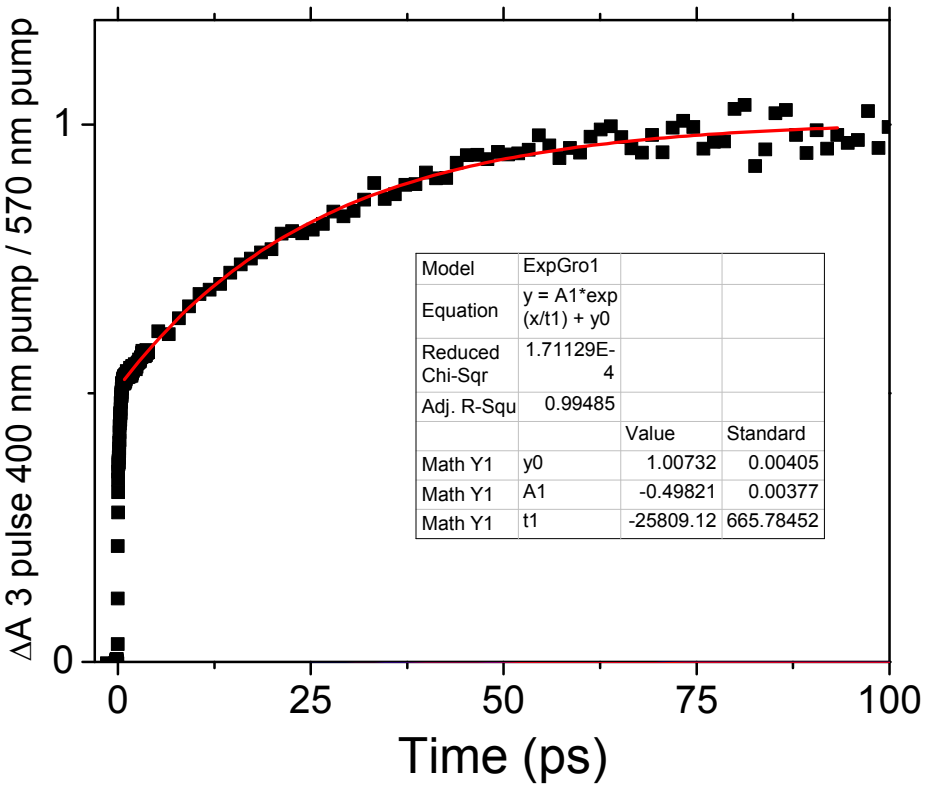

Figure S1: Plot of band edge bleach ratio between the three pulse experiments where the pump wavelength was 400 nm and 570 nm. The saturation pulse for both the cases was an intense 400 nm pulse. This division factors out the effects of Auger Recombination isolating the bleach rise due to spin flipping. Red curve is a fit to a mono-exponential rise of nearly 26 ps.

Experimental determination of absorption cross section of the CdSe/CdS core/shell nanocrystals:

The absorption cross section of the CdSe/CdS core/shell QDs was experimentally determined according to previously reported procedure.[24] Figure S1A demonstrates the 1Se-1Sh transition bleach as a function of pump-probe delay after 400 nm excitation, for a series of different excitation photon fluxes as indicated in the inset. All these experiments were carried out with weak excitation fluences such that the bleach changes linearly. Figure S1B shows a plot of $\Delta I/I_0$ vs. photon flux

change. From the linear fit of these experimental data points and known the 2-fold degeneracy of 1S1S transition of the CdSe dots, the slope of the fit gives the absorption cross section value at the pump wavelength, $\sigma_{400}=(2.7\pm0.1)\times10^{-15}$ cm^2.

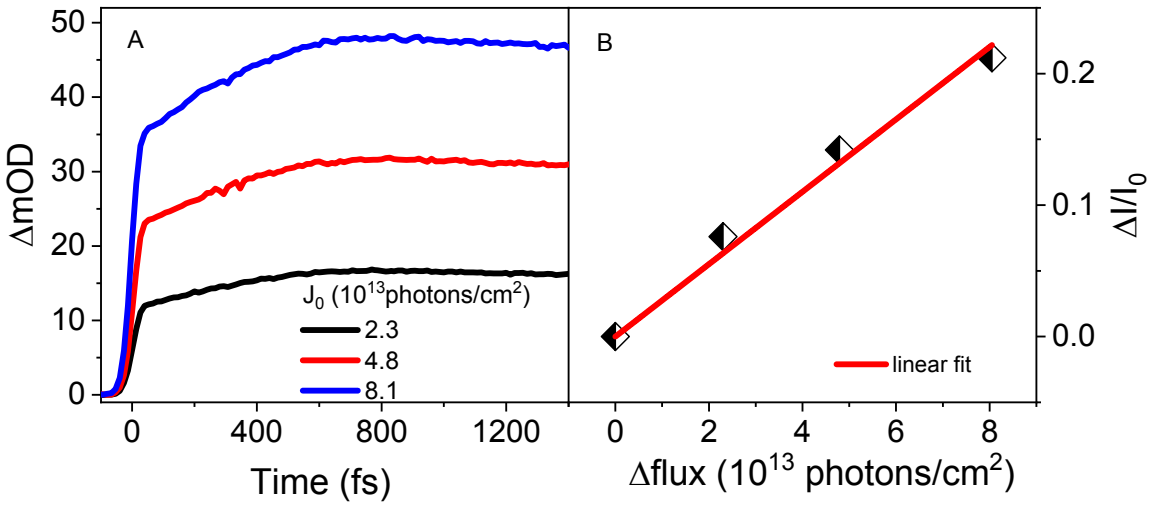

Figure S2: Determination of absorption cross section of CdSe/CdS core/shell nanocrystals. (A) Plot of 1S1S bleach signal (at 570 nm) vs. pump-probe delay (up to 1.4 ps) after excitation with 400 nm pulses, at different excitation pump fluences as presented in the inset; (B) Plot of fractional absorption change vs. photon flux and linear fit of the experimental data. The absorption cross section can be calculated from the slope of this fit.

Simulating pump fluence dependence of the band edge bleach

Defining J_0 and J_∞ as the pump photon flux (photons/cm^2) at the front and back surfaces of an optically thick sample cell, and σ as the absorption cross section (cm^2) at the pump wavelength, the average no. of absorbed photons per nanocrystals at the front (η_0) and back surface (η_∞) are:

$$J_0\sigma = \eta_0 \quad \text{and} \quad J_\infty\sigma = \eta_\infty.$$

ρ_T , the total density/cm^2 of NC in the sample, assuming pump wavelength absorption is unaffected by existing excitons, is given in terms of η_0, η_∞ *and* σ*:*

$$e^{-\sigma\rho_T} = \frac{\eta_\infty}{\eta_0} \rightarrow \rho_T = \frac{1}{\sigma}\ln\left(\frac{\eta_0}{\eta_\infty}\right) = \frac{1}{\sigma}\int_{\eta_\infty}^{\eta_0}\frac{1}{\eta}\mathrm{d}\eta \tag{S1}$$

For an optically thin slab of nano-dots the probability for a quantum dot to absorb N pump photons follows the Poisson distribution,

$$P_N = \frac{e^{-\eta}(\eta)^N}{N!} \text{ where } \sum_{N=0}^{\infty} P_N = 1 \text{ and } P_0 = e^{-\eta}$$

Accordingly, the probability of absorbing *at all* at η is given by $P_{N>0} = 1 - e^{-\eta}$, and the probability of absorbing more than one photon per nanocrystals is given by, $P_{N>1} = 1 - e^{-\eta} - \eta\, e^{-\eta}$.

Returning to an optically thick sample where pump intensity reduces significantly over the cell, all the above can be used to calculate the density per unit area of particles which have absorbed N pump photons as:

$$\rho_N = \int_{\eta_0}^{\eta_\infty}\frac{e^{-\eta}(\eta)^{(N-1)}\mathrm{d}\eta}{N!\quad\sigma} = \int_{\eta_\infty}^{\eta_0} d\rho_N(\eta) \tag{S2}$$

Finally before deriving expressions for the fractional BE bleach we require two more densities, $\rho_{N>0}$ the density per unit area of dots absorbing any number of photons, and $\rho_{N>1}$ the differential density of those absorbing two or more:

$$\rho_{N>0} = \int_{\eta_\infty}^{\eta_0}\frac{1 - e^{-\eta}\mathrm{d}\eta}{\eta\quad\sigma} \tag{S3}$$

And

$$\rho_{N>1} = \frac{1}{\sigma}\int_{\eta_\infty}^{\eta_0} \frac{1 - e^{-\eta} - \eta e^{-\eta}}{\eta} \mathrm{d}\eta \tag{S4}$$

To derive an expression for the intensity dependent fractional bleaching at the band edge (BE) we use the equations for $\rho_T, \rho_{N>0}$ and $\rho_{N>1}$ $along\ with\ \eta_\infty, \eta_0, and\ \sigma_{BE}$ the cross section at the first exciton peak. Notice that when pumping high in the inter-band continuum, σ is often more than 10 times larger than σ_{BG}. Assuming linear bleaching of the BE transition up to a degeneracy of 2, α_{BE} the sample band edge absorbance after excitation (and carrier cooling) α_{BE,η_0} is obtained by integrating over the pump fluences throughout the cell:

$$\alpha_{BE,\eta_0} = \left[\rho_T - {}^{\rho_{N>0}}\!/_{2} - {}^{\rho_{N>1}}\!/_{2}\right]\sigma_{BE}$$

The fraction of residual absorption after pump excitation is accordingly,

$$\frac{\alpha_{BE,\eta_0}}{\alpha_{BE}} = \frac{2\rho_T - \rho_{N>0} - \rho_{N>1}}{2\rho_T} \tag{S5}$$

Substituting S1, S3, and S4 into equation S5:

$$\frac{\alpha_{BE,\,\eta_0}}{\alpha_{BE}} = \frac{1}{[\ln|\eta|]_{\eta_\infty}^{\eta_0}}\int_{\eta_\infty}^{\eta_0} \frac{e^{-\eta} + 0.5\eta e^{-\eta}}{\eta} \mathrm{d}\eta \tag{S6}$$

Finally the BE fractional bleach completes the fraction in equation S6 to one, leading to:

$$\frac{\Delta\alpha_{BE,\,\eta}}{\alpha_{BE}} = 1 - \frac{1}{[\ln|\eta|]_{\eta_\infty}^{\eta_0}}\int_{\eta_\infty}^{\eta_0} \frac{e^{-\eta} + 0.5\eta e^{-\eta}}{\eta} \mathrm{d}\eta \tag{S7}$$

which has been used to simulate the plot of ${}^{\Delta\alpha}\!/_{\alpha_0}$ vs. η_0 in Figure 5B of the manuscript.

Theoretical Model

We assume that the electron states exhibit a separate ground state S^e, $800cm^{-1}$ below a group of three excited electron states $P^e_{0,\pm 1}$. The splitting between the p-states is on the order of $2\Delta = 100\ c\ m^{-1}$. We have also performed a TDDFT calculation and estimated various spin-orbit couplings between excited states. Because of the multitude of hole states there is not one number, but a spectrum of couplings, spanning a range of $s = 10 - 300cm^{-1}$.

In Figure **S2** we describe our model for the experiment in CdSe NCs. There are two excitons, one is "cold", in the band edge, due to the first experimental pulse with an up-spin electron in the S^e state and the second has its hole at the top of the valence manifold but its up-spin electron is in one of the P states and it is blocked from further decay onto the S^e level because of Pauli exclusion.

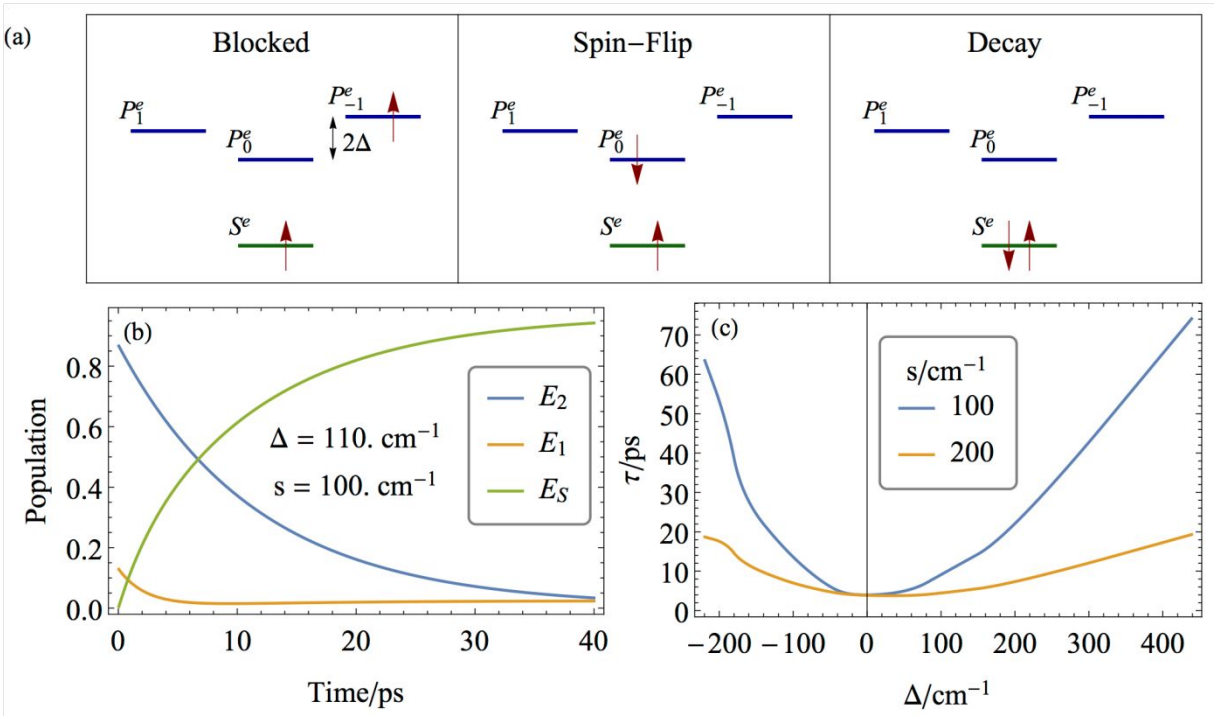

Figure S2: (a) Left panel: the up-spin electron in the $\boldsymbol{P^e_{-1\uparrow}}$ level (say) is *blocked* from decay into the edge level $\boldsymbol{S^e_{\updownarrow}}$ due to Pauli exclusion. Middle panel: A spin-orbit induced spin-flip occurs: $\boldsymbol{P^e_{-1\uparrow} \rightarrow P^e_{0\downarrow}}$. Right panel: The down-spin electron decay $\boldsymbol{P^e_{0\downarrow} \rightarrow S^e_{\updownarrow}}$. (b) The populations of the three adiabatic states as a function

of time for the indicated values of $\boldsymbol{\Delta}$ and $\boldsymbol{s}$. (c) a sensitivity analysis checking time scale for the final cooling to the parameters.

a) Dissipative dynamics under spin-flip

We first neglect spin-orbit coupling. In this case, we consider the electronic Hamiltonian of the levels $P^e_{-1\uparrow}$, $P^e_{0\downarrow}$ and $S^e_{\downarrow}$:

$$H_S = \begin{pmatrix} 2\Delta & 0 & 0 \\ 0 & 0 & 0 \\ 0 & 0 & -\epsilon_S \end{pmatrix} \tag{S8}$$

Where we assumed that the energy of the $P^e_{0\downarrow}$ level is zero and that of the $P^e_{-1\uparrow}$ level is displaced by 2Δ while that of the $S^e_{\downarrow}$ is below by $\epsilon_S > 0$.

The total Hamiltonian H_{tot} describing the coupling of the system to a bath of phonons is

$$H_{tot} = H_B + H_S + \sum_j \left(\frac{p_j}{m_j}\right) \begin{pmatrix} 0 & 0 & 0 \\ 0 & 0 & A_j^{12} \\ 0 & A_j^{21} & 0 \end{pmatrix} \tag{S9}$$

where $A_j^{12} = A_j^{21\,*}$ are the non-adiabatic coupling terms and

$$H_B = \sum_j \left(\frac{p_j^2}{2m_j} + \frac{1}{2} m_j \omega_j^2 x_j^2\right) \tag{S10}$$

is the phonon Hamiltonian. Notice that there is no non-adiabatic coupling of the $P^e_{-1\uparrow}$ level and the $S^e_{\downarrow}$ level because of the different spins.

Now, introduce the spin coupling s between levels $P^e_{-1\uparrow}$ and $P^e_{0\downarrow}$. The 3-level Hamiltonian in Eq. (S8) is thus generalized to

$$H_S = \begin{pmatrix} 2\Delta & s & 0 \\ s & 0 & 0 \\ 0 & 0 & -\epsilon_S \end{pmatrix} \tag{S11}$$

We diagonalize $H_a = U^\dagger H_S U$, using

$$U = \begin{pmatrix} \cos\theta/2 & -\sin\theta/2 & 0 \\ \sin\theta/2 & \cos\theta/2 & 0 \\ 0 & 0 & 1 \end{pmatrix} \tag{S12}$$

giving:

$$H_a \equiv \begin{pmatrix} E_1 & 0 & 0 \\ 0 & E_2 & 0 \\ 0 & 0 & E_S \end{pmatrix} = 2R \begin{pmatrix} \cos^2\theta/2 & 0 & 0 \\ 0 & -\sin^2\theta/2 & 0 \\ 0 & 0 & -\epsilon/2R \end{pmatrix} \tag{S13}$$

Where R and θ are defined by requiring $\Delta = R\cos\theta$ and $s = R\sin\theta$. The total Hamiltonian then becomes:

$$H_{tot}^{a} = H_a + H_B + \sum_j \left(\frac{p_j}{m_j}\right) \begin{pmatrix} 0 & 0 & \tilde{A}_j^{02} \\ 0 & 0 & \tilde{A}_j^{12} \\ \tilde{A}_j^{20} & \tilde{A}_j^{21} & 0 \end{pmatrix} \tag{S14}$$

where $\tilde{A}_j^{12} = \tilde{A}_j^{21\,*} = A_j^{12}\cos\theta/2$ and $\tilde{A}_j^{02} = \tilde{A}_j^{20\,*} = A_j^{12}\sin\theta/2$ now couple both adiabatic P-states with S-states because the spin-orbit coupling mixes the up- and down-spin states.

In order to study the dynamics, we assume the reduced 3×3 density matrix σ_{ij} obeys the Lindblad equation[33]:

$$\dot{\sigma}(t) = -\frac{i}{\hbar}[H_a + H_{1a,\sigma}] + \mathfrak{D}\,\sigma(t) \tag{S15}$$

where the dissipative and hermitian bath effects are given as:

$$\mathfrak{D}\,\sigma = \sum_{\omega} \gamma(\omega)\left[L(\omega)\sigma L(\omega)^{\dagger} - \frac{1}{2}\{L(\omega)L(\omega)^{\dagger}, \sigma\}\right] \tag{S16}$$

$$H_1 = \sum_{\omega} S(\omega) L(\omega)^{\dagger} L(\omega) \tag{S17}$$

where the summation is over discrete frequencies, $\omega_m = \mathrm{m}2\pi/\mathrm{T_d}$ where T_d is the discretization period and

$$\Gamma(\omega) = \frac{1}{2}\gamma(\omega) + iS(\omega) = \int_0^{T_d} e^{i\omega t} \left\langle \frac{p(t)p(0)}{m \quad m} \right\rangle_{\beta} dt \tag{S18}$$

is the bath frequency velocity autocorrelation function at inverse temperature β (see Appendix A). For the two resonant frequencies, $\hbar\omega_{20} = \varepsilon_S + 2R\cos^2\theta/2$ and $\hbar\omega_{21} = \varepsilon_S - 2R\sin^2\theta/2$ present in our Hamiltonian, we have the following Lindblad operator

$$L_{\omega} = \hbar^{-1} \begin{pmatrix} 0 & 0 & \tilde{A}_j^{02}\delta_{-\omega,\omega_{20}} \\ 0 & 0 & \tilde{A}_j^{12}\delta_{-\omega,\omega_{21}} \\ \tilde{A}_j^{20}\delta_{-\omega,\omega_{20}} & \tilde{A}_j^{21}\delta_{-\omega,\omega_{21}} & 0 \end{pmatrix} \tag{S19}$$

which is a Liouvillian eigenstate $[H,L_\omega] = \hbar\omega\, L_\omega$. With this, the dissipation above term in eq. (S16) becomes

$$\mathfrak{D}\,\sigma = \begin{pmatrix} -D_{20}\sigma_{00} + D_{02}\sigma_{22} & -\frac{D_{20}+D_{21}}{2}\sigma_{01} & -\frac{D_{20}+D_{02}+D_{12}}{2}\sigma_{02} \\ -\frac{D_{20}+D_{21}}{2}\sigma_{10} & -D_{21}\sigma_{11} + D_{12}\sigma_{22} & -\frac{D_{02}+D_{12}+D_{21}}{2}\sigma_{12} \\ -\frac{D_{20}+D_{02}+D_{12}}{2}\sigma_{20} & -\frac{D_{02}+D_{12}+D_{21}}{2}\sigma_{21} & -(D_{02}+D_{12})\sigma_{22} + D_{20}\sigma_{00} + D_{21}\sigma_{11} \end{pmatrix}$$

where

$$D_{02} = a\omega_{02}\big(\langle n\rangle_{\beta\hbar\omega_{02}} + 1\big)\sin^2\theta/2$$
$$D_{20} = a\omega_{02}\langle n\rangle_{\beta\hbar\omega_{02}}\sin^2\theta/2$$
$$D_{12} = a\omega_{12}\big(\langle n\rangle_{\beta\hbar\omega_{12}} + 1\big)\cos^2\theta/2$$
$$D_{21} = a\omega_{12}\langle n\rangle_{\beta\hbar\omega_{12}}\cos^2\theta/2$$

with $a = T_d\,\frac{|A_{12}|^2}{2m\hbar}$ the dimensionless non-adiabatic parameter.

b) Why spin-flip Auger coupling is weak

In CdSe NCs Auger coupling is a major nonradiative energy dissipation mechanism in excited NCs (11). The direct coupling between excitons involves the matrix elements:

$$\langle 0 \,|\, c_{j\uparrow}^\dagger c_{b\uparrow}\hat{V}c_{a\uparrow}^\dagger c_{i\uparrow} \,|\, 0\rangle = \delta_{ij}\delta_{ab}2(2V_{vssv} - V_{svsv})n_s n_v + 2\delta_{ij}(2V_{btta} - V_{btat})n_t - 2\delta_{ab}(2V_{ittj} - V + 2(V_{ibja} - V_{ibaj}) \quad \text{(S20)}$$

where $\hat{V} = \sum_{stuv}\sum_{\sigma\sigma'=\uparrow\downarrow} V_{utsv}\, c_{u\sigma}^\dagger c_{t\sigma'}^\dagger c_{s\sigma} c_{v\sigma}$ is the Coulomb interaction in second quantization, $\psi_s(\boldsymbol{r})$, $\psi_t(\boldsymbol{r})$, $\psi_u(\boldsymbol{r})$, $\psi_v(\boldsymbol{r})$ are one-electron (Hartree-Fock) eigenstates and

$$V_{utsv} = \frac{1}{2}\iint \frac{[\psi_u(\boldsymbol{r}')\psi_v(\boldsymbol{r}')][\psi_t(\boldsymbol{r})\psi_s(\boldsymbol{r})]}{|\boldsymbol{r}-\boldsymbol{r}'|} d\boldsymbol{r}d\boldsymbol{r}' \quad \text{(S21)}$$

and for which the creation and annihilation commutation relations are:

$$\left[c_{u\sigma}^\dagger, c_{s\sigma'}\right]_+ = \delta_{\sigma\sigma'}\delta_{uv} \quad \text{(S22)}$$

The first term in eq. (S20), $i = j$ and $a = b$ is a "diagonal element" and is not interesting for our purpose. When either $a = b$ or $i = j$ (but not both) it's the second (or third) term that is important. Than either the electron changes state while the hole is a spectator or vice versa. Suppose it's the

electron changing from a to b while the hole stays put in $i = j$, the coupling then involves the Coulomb interaction of an electron charge distribution $2\psi_b(\boldsymbol{r})\psi_a(\boldsymbol{r})$ with the *entire* electron density $2\sum_{i=1}^{N_e/2}|\psi_i(\boldsymbol{r})|^2$ in the nanocrystals (corrected by a much smaller exchange term, since only ψ_t's that overlap with both ψ_a and ψ_b contribute). So, as long as $\psi_a(\boldsymbol{r})$ and $\psi_b(\boldsymbol{r})$ strongly overlap in space this is very strong.

However, if the coupling involves spin-flip, the corresponding Auger element evaluates just one term

$$\langle 0 \,|\, c_{j\downarrow}^{\dagger} c_{b\downarrow} \hat{V} c_{a\uparrow}^{\dagger} c_{i\uparrow} \,|\, 0 \rangle = 2V_{biaj} \qquad \text{(S23)}$$

which is the Coulomb interaction between two charge distributions one is $\psi_b(\boldsymbol{r})\psi_j(\boldsymbol{r})$ and the other $\psi_i(\boldsymbol{r})\psi_j(\boldsymbol{r})$, for this to be strong one requirement is good electron-hole overlap for each of the two excitons and that they are reasonably close so that the Coulomb interaction is considerable. The direct Auger involves interacting of the dynamical electron with all other electrons in the system while the spin-flip process is just a local two-electron interaction.

Summarizing, Auger processes which are typically efficient mechanisms for biexciton decay in nanocrystals are much slower when a spin-flip is involved.

c) Results of model

The model involves 5 parameters: the temperature T, taken to be 300K, energy offset of the $S_{\downarrow}^{e}$ state ε_S with respect to the P_e^0 state, the dimensionless non-adiabatic coupling strength a, the P-level splitting Δ and the spin-flip coupling strength s.

Using Q-CHEM (35) we have performed *ab initio* calculations on relaxed $Cd_{36}Se_{36}$ (see Ref. 34). We used the PW91 functional and a small basis set (STO-3G). The calculations reveal the typical CdSe NC frontier orbital structure: a dense manifold of hole states and a sparse one for electron states above it, with an optical gap, of 1.1eV. We also determined from the calculation $\varepsilon_S = 0.1\ eV$ and $\Delta = 500\ \mu E_h$. Finally we determined the parameter $a = 0.14$, by requiring that the rate of decay $P \rightarrow S$ without a spectator (without the requirement for spin-flip) be 0.5 ps, in accordance with the known experiment estimates.

The spin-flip mechanism considered here is caused by the spin-orbit coupling between a pair of singlet and triplet excitons. The singlet exciton, originally formed by the laser pulse, has decayed in a fast time scale to the blocked state, where the electron is in a P^e excited state with the spin. The triplet exciton is similar except that the excited P^e electron has flipped its spin (and changed to a different P^e state, see **Figure S2**). Due to the large density of hole states in our model $Cd_{36}Se_{36}$ system, we were forced to produce a large number of exciton states: the electron in the first 35 excitons was in the lowest S^e state and only the hole was in an excited state and only in exciton

number 36, at energy of 1.34eV, was the first to have an electron in an excited P^e state . Out of the first 200 excitons we selected the few that were 1) dominated by a single electron-hole excitation, and 2) the electron was in one of the two lowest diabatic P^e states. Due to non-adiabatic effects these states mix slightly and we label the adiabatic states as 1 (mostly P^e_0) and 2 (mostly P^e_{-1}). We focused attention on a small energy band 1.34-1.56eV which contained about 100 excitons (out of the 200 calculated). Of those, only nine were singlet excitons, four with the electron in state 1 and five with the electron in state 2. We also identified sixteen such triplet excitons, nine having an electron in state 1 and seven an electron in state 2. Within these excitons there are four types of SO couplings: $\langle S_1 | H_{SO} | T_1 \rangle$, $\langle S_2 | H_{SO} | T_2 \rangle$, $\langle S_1 | H_{SO} | S_2 \rangle$ and $\langle S_2 | H_{SO} | S_1 \rangle$. The first pair of matrix elements describe a hole spin-flip (the electron stays put) while the second pair describe an electron spin-flip. The calculations show, that the hole spin-flip (which is not of interest for our mechanism) involved a strong coupling averaging at $200\ cm^{-1}$ and peaking at $480\ cm^{-1}$. On the other hand, electron spin-flip SO couplings typically have 5 times weaker couplings: averaging at $50\ cm^{-1}$ and peaking at $144\ cm^{-1}$. These calculated ab initio values prompted us to take a representative value of $s = 100\ cm^{-1}$ and then also comparing to $s = 200\ cm^{-1}$ as a stability analysis.

With these parameters we solved the Lindblad equation and taking (see **Figure S2** (a)) and obtained the adiabatic state populations $\sigma_{ii}(t),\ i = 2,1,S^e$. The system starts in (diabatic) state P^e_{-1} which populates mainly state 2 and due to spin-orbit coupling also a bit of state 2 (this small part decays faster to the S^e state). Then the main part of the population decays at a time scale of 10 ps, reaching equilibrium.

We also checked the sensitivity of the results to s and Δ and obtained the lifetime in Figure S2 (c). It is interesting to see that for large spin-orbit couplings such as $200\ cm^{-1}$, the spin-flip effect slows down to about 5 ps.

Appendix A: Harmonic Correlation Function

The time correlation function of the Harmonic Oscillator at temperature β is

$$C(t,\beta) = \frac{1}{m^2}\sum_n \frac{e^{-\beta E_n}}{Z} \langle n|\hat{p}(t)\hat{p}(0)|n\rangle \tag{S24}$$

$$= \frac{1}{m^2}\sum_{nm} \frac{e^{-\beta E_n}}{Z}\, e^{iE_{nm}t} \langle n|\hat{p}|m\rangle\langle m|\hat{p}|n\rangle \tag{S25}$$

$$= \frac{1}{m^2}\sum_{nm}\frac{e^{-\beta E_n}}{Z}e^{iE_{nm}t}|\langle n|\hat{p}|m\rangle|^2 \tag{S26}$$

where $M\hbar = P^2 t$

$$Z(\beta) = \sum_{n=0}^{\infty} e^{-\beta\hbar\omega n} = \frac{1}{1-e^{-\beta\hbar\omega}} \tag{S27}$$

$$\langle n|\hat{p}|m\rangle = i\sqrt{\frac{\hbar m\omega}{2}}\langle n|\hat{a}^{\dagger} - \hat{a}|m\rangle \tag{S28}$$

$$= i\sqrt{\frac{\hbar m\omega}{2}}\left(\sqrt{m+1}\,\delta_{n,m+1}\sqrt{m}\delta_{n,m-1}\right) \tag{S29}$$

Hence

$$|\langle n|\hat{p}|m\rangle|^2 = \frac{m\hbar\omega}{2}((m+1)\delta_{n,m+1} + m\delta_{n,m-1}) \tag{S30}$$

$$C(t,\beta) = \frac{\hbar\omega}{2m}\left(e^{i\omega t} + e^{-i\omega t}e^{\beta\hbar\omega}\right)\frac{1}{Z}\sum_{n=0}^{\infty} ne^{-\beta n\hbar\omega} \tag{S31}$$

$$= \frac{\hbar\omega}{2m}\left(e^{i\omega t} + e^{-i\omega t}e^{\beta\hbar\omega}\right)\langle n\rangle_{\beta} \tag{S32}$$

And

$$\langle n\rangle_{\beta,\omega} = \frac{1}{Z}\sum_{n=0}^{\infty} ne^{-\beta n\hbar\omega} \tag{S33}$$

$$= -\frac{1}{\hbar\omega}\frac{\partial}{\partial\beta}\ln Z \tag{S34}$$

$$= \frac{1}{\hbar\omega}\frac{\partial}{\partial\beta}\ln\left(1 - e^{-\beta\hbar\omega}\right) \quad \text{(S35)}$$

$$= \frac{1}{e^{\beta\hbar\omega} - 1} \quad \text{(S36)}$$

Clearly

$$\langle n\rangle_{\beta,\omega} + 1 = e^{\beta\hbar\omega}\langle n\rangle_{\beta,\omega} \quad \text{(S37)}$$

finally,

$$C(t,\beta) = \frac{\hbar\omega}{2m}\langle n\rangle_{\beta\omega}\left(e^{i\omega t} + e^{-i\omega t}e^{\beta\hbar\omega}\right) \quad \text{(S38)}$$

$$= \frac{\hbar\omega}{2m}\left(\langle n\rangle_{\beta\omega}e^{i\hbar\omega t} + e^{-i\hbar\omega t}\left(\langle n\rangle_{\beta\omega} + 1\right)\right) \quad \text{(S39)}$$

if we assume that the frequency is discrete $\omega_m = \frac{2\pi}{T_d}m$ where m is integer then the response function of eq. (S18) assumes the following form:

$$\gamma(\pm\omega,\beta) = T_d\frac{\hbar\omega}{2m}\left(\langle n\rangle_{\beta\omega} + \frac{1 \pm 1}{2}\right)$$

Appendix B: $Cd_{36}Se_{36}$ Input file

```
$molecule
0 1
Cd 2.26266696 0.80336407 -6.46510988
Cd 2.26266696 0.80336407 6.46510988
Cd -0.43389281 -2.49625428 -6.40155700
Cd -0.43389281 -2.49625428 6.40155700
Cd -1.88543621 1.45902174 -6.49895678
Cd -1.88543621 1.45902174 6.49895678
Cd -4.10780789 -1.20308722 -4.75283647
Cd -4.10780789 -1.20308722 4.75283647
Cd 0.83699863 4.07573258 -4.85280032
Cd 0.83699863 4.07573258 4.85280032
Cd 3.09910097 -2.83326887 -4.78577050
Cd 3.09910097 -2.83326887 4.78577050
Cd 2.83458308 0.82682770 -2.31844206
Cd 2.83458308 0.82682770 2.31844206
Cd -0.68852828 -3.06559991 -2.27167782
Cd -0.68852828 -3.06559991 2.27167782
Cd -2.12214994 1.94667024 -2.34781506
Cd -2.12214994 1.94667024 2.34781506
Cd -4.03854179 -1.39280936 0.00000000
Cd 3.40396851 -2.47907728 0.00000000
Cd 0.34766961 4.16957255 0.00000000
Cd 5.42916889 3.32370962 0.00000000
Cd -5.60011141 3.27040539 0.00000000
Cd 0.37762859 -6.53714690 0.00000000
Cd 4.57345019 3.90346038 -4.31177363
```

```
Cd 4.57345019 3.90346038 4.31177363
Cd -5.68257664 2.23505087 -4.30733764
Cd -5.68257664 2.23505087 4.30733764
Cd 1.23344351 -6.03770026 -4.29679356
Cd 1.23344351 -6.03770026 4.29679356
Cd 3.23078991 6.19612775 -2.10464336
Cd 3.23078991 6.19612775 2.10464336
Cd -7.18687857 0.06708793 -2.12106907
Cd -7.18687857 0.06708793 2.12106907
Cd 3.90521114 -5.97673874 -2.11084867
Cd 3.90521114 -5.97673874 2.11084867
Se -1.50427559 -4.48878986 0.00000000
Se 4.45358377 0.70162186 0.00000000
Se -2.80571365 3.38671429 0.00000000
Se 1.48190896 6.73882226 0.00000000
Se -6.81740331 -1.70124355 0.00000000
Se 5.16109123 -4.67106092 0.00000000
Se -2.63307265 -0.89017218 -2.35055978
Se -2.63307265 -0.89017218 2.35055978
Se 0.64055415 2.65897350 -2.37385332
Se 0.64055415 2.65897350 2.37385332
Se 1.95497191 -1.90482171 -2.34921571
Se 1.95497191 -1.90482171 2.34921571
Se 1.68463259 -7.73753003 -2.14176246
Se 1.68463259 -7.73753003 2.14176246
Se 5.83081241 5.07118510 -2.12602700
Se 5.83081241 5.07118510 2.12602700
Se -7.32389824 2.89605112 -2.15331364
Se -7.32389824 2.89605112 2.15331364
Se -1.08500310 -4.57016641 -4.66077668
Se -1.08500310 -4.57016641 4.66077668
Se 4.38648158 1.17716053 -4.69347086
Se 4.38648158 1.17716053 4.69347086
Se -3.14171439 3.20684327 -4.70192993
Se -3.14171439 3.20684327 4.70192993
Se 2.74601892 6.05192643 -4.87800129
Se 2.74601892 6.05192643 4.87800129
Se -6.73130484 -0.37782115 -4.85442287
Se -6.73130484 -0.37782115 4.85442287
Se 3.98914709 -5.42724163 -4.87277230
Se 3.98914709 -5.42724163 4.87277230
Se -2.72602690 -1.09340696 -7.16667357
Se -2.72602690 -1.09340696 7.16667357
Se 0.45328051 2.74250861 -7.26553396
Se 0.45328051 2.74250861 7.26553396
Se 2.14166044 -1.86454113 -7.21620233
Se 2.14166044 -1.86454113 7.21620233
$end
$rem
JOBTYPE sp
SCF_FINAL_PRINT 1
SCF_CONVERGENCE 6
PRINT_ORBITALS 1000
MOLDEN_FORMAT TRUE
basis gen
exchange PW91
SCF_ALGORITHM diis_gdm
CIS_N_ROOTS 100
CIS_SINGLETS true
CIS_TRIPLETS true
CIS_CONVERGENCE 6
CALC_SOC true
SYMMETRY false
```

```
UNRESTRICTED false
SYM_IGNORE true
max_scf_cycles 500
mem_total 200000
mem_static 2000
$end
$basis
Se 0
S 3 1.00
2480.6268140 0.1543289673
451.8492708 0.5353281423
122.2880464 0.4446345422
SP 3 1.00
206.1578780 -0.0999672292 0.1559162750
47.90665727 0.3995128261 0.6076837186
15.58073180 0.7001154689 0.3919573931
SP 3 1.00
17.63999414 -0.2277635023 0.0049515112
5.380760465 0.2175436044 0.5777664691
2.076064666 0.9166769611 0.4846460366
SP 3 1.00
1.2146442970 -0.3088441215 -0.1215468600
0.4482801363 0.0196064117 0.5715227604
0.1979652346 1.1310344420 0.5498949471
D 3 1.00
17.63999414 0.2197679508
5.380760465 0.6555473627
2.076064666 0.2865732590
****
Cd 0
S 3 1.00
4950.2619050 0.1543289673
901.6963856 0.5353281423
244.0342313 0.4446345422
SP 3 1.00
433.4469385 -0.0999672292 0.1559162750
100.7237469 0.3995128261 0.6076837186
32.75848861 0.7001154689 0.3919573931
SP 3 1.00
52.59279235 -0.2277635023 0.0049515111
16.04247800 0.2175436044 0.5777664691
6.189686744 0.9166769611 0.4846460366
SP 3 1.00
5.674851796 -0.3306100626 -0.1283927634
2.209757875 0.0576109533 0.5852047641
0.9727408566 1.1557874500 0.5439442040
SP 3 1.00
0.5949150981 -0.3842642607 -0.3481691526
0.3203250000 -0.1972567438 0.6290323690
0.1414931855 1.3754955120 0.6662832743
D 3 1.00
52.59279235 0.2197679508
16.04247800 0.6555473627
6.189686744 0.2865732590
D 3 1.00
3.642963976 0.1250662138
1.418551290 0.6686785577
0.6244497700 0.3052468245
****
$end
```